Magnetic Resonance Imaging 62 (2019) 78–86

Contents lists available at ScienceDirect

Magnetic Resonance Imaging

journal homepage: www.elsevier.com/locate/mri

Original contribution

Dynamic contrast-enhanced MRI to assess hepatocellular carcinoma response to Transarterial chemoembolization using LI-RADS criteria: A pilot study

Alana Thibodeau-Antonacci[a,b], Léonie Petitclerc[a,b], Guillaume Gilbert[c], Laurent Bilodeau[a], Damien Olivié[a], Milena Cerny[a,b], Hélène Castel[d], Simon Turcotte[b,e], Catherine Huet[a], Pierre Perreault[a], Gilles Soulez[a], Miguel Chagnon[f], Samuel Kadoury[a,b,g], An Tang[a,b,*]

[a] Department of Radiology, Centre hospitalier de l'Université de Montréal (CHUM), Montréal, QC, Canada
[b] Centre de recherche du Centre hospitalier de l'Université de Montréal (CRCHUM), Montréal, QC, Canada
[c] MR Clinical Science, Philips Healthcare, Canada
[d] Department of Hepatology and Liver transplantation, Centre hospitalier de l'Université de Montréal (CHUM), Montréal, QC, Canada
[e] Department of Surgery, Hepatopancreatobiliary and Liver Transplantation Service, Centre hospitalier de l'Université de Montréal (CHUM), Montréal, QC, Canada
[f] Department of Mathematics and Statistics, Université de Montréal, QC, Canada
[g] École Polytechnique, Montréal, Québec, Canada

A B S T R A C T

Purpose: To identify quantitative dynamic contrast-enhanced (DCE)-MRI perfusion parameters indicating tumor response of hepatocellular carcinoma (HCC) to transarterial chemoembolization (TACE).

Materials and methods: This prospective pilot study was approved by our institutional review board; written and informed consent was obtained for each participant. Patients underwent DCE-MRI examinations before and after TACE. A variable flip-angle unenhanced 3D mDixon sequence was performed for T1 mapping. A dynamic 4D mDixon sequence was performed after contrast injection for assessing dynamic signal enhancement. Nonparametric analysis was conducted on the time-intensity curves. Parametric analysis was performed on the time-concentration curves using a dual-input single-compartment model. Treatment response according to Liver Reporting and Data System (LI-RADS) v2018 was used as the reference standard. The comparisons within groups (before vs. after treatment) and between groups (nonviable vs. equivocal or viable tumor) were performed using nonparametric bootstrap taking into account the clustering effect of lesions in patients.

Results: Twenty-eight patients with 52 HCCs (size: 10–104 mm) were evaluated. For nonviable tumors ($n = 27$), time to peak increased from 62.5 ± 18.2 s before to 83.3 ± 12.8 s after treatment ($P < 0.01$). For equivocal or viable tumors ($n = 25$), time to peak and mean transit time significantly increased (from 54.4 ± 24.1 s to 69.5 ± 18.9 s, $P < 0.01$ and from 14.2 ± 11.8 s to 33.9 ± 36.8 s, $P = 0.01$, respectively) and the transfer constant from the extracellular and extravascular space to the central vein significantly decreased from 14.8 ± 14.1 to 8.1 ± 9.1 s^{-1} after treatment ($P = 0.01$).

Conclusion: This prospective pilot DCE-MRI study showed that time to peak significantly changed after TACE treatment for both groups (nonviable tumors and equivocal or viable tumors). In our cohort, several perfusion parameters may provide an objective marker for differentiation of treatment response after TACE in HCC patients.

Abbreviations: ART, Arterial fraction; DCE-MRI, Dynamic contrast-enhanced MRI; DV, Distribution volume; FOV, Field of view; HCC, Hepatocellular carcinoma; LI-RADS, Liver Imaging Reporting and Data System; LR-TR, LI-RADS treatment response; MTT, Mean transit time; nMITR, Normalized maximum intensity time ratio; PER, Peak enhancement ratio; TACE, Transarterial chemoembolization; TE, Echo time; TR, Repetition time; TTP, Time to peak

* Corresponding author at: Department of Radiology, Radio-oncology and Nuclear Medicine, University of Montreal and CRCHUM, 900, rue Saint-Denis, Montréal, Québec, H2X 0A9, Canada.

E-mail address: an.tang@umontreal.ca (A. Tang).

https://doi.org/10.1016/j.mri.2019.06.017
Received 8 March 2019; Received in revised form 5 June 2019; Accepted 23 June 2019

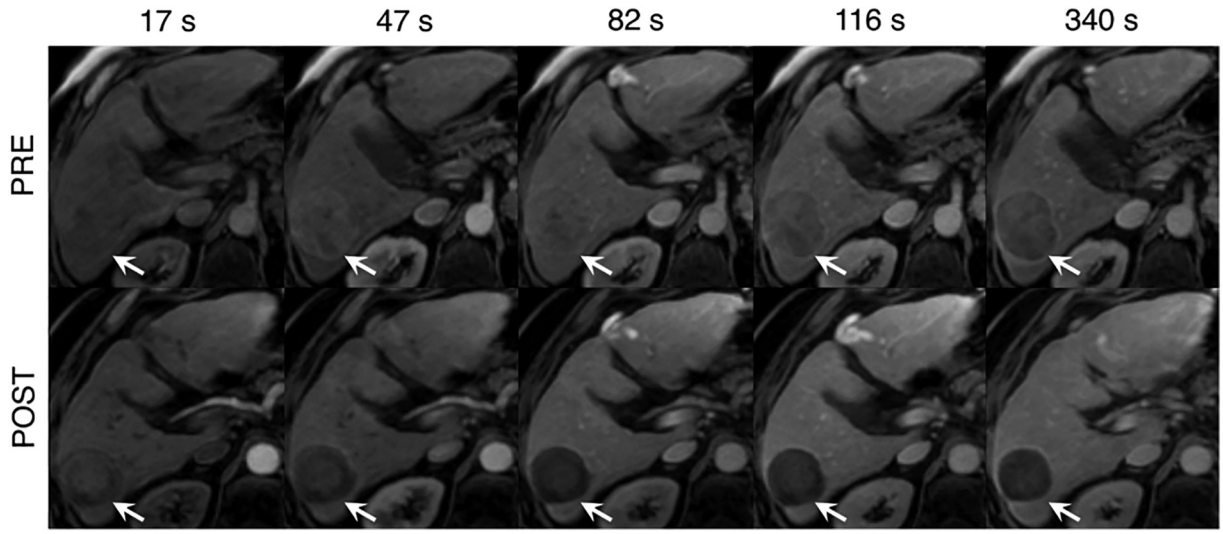

Fig. 1. 66-year-old man with HCC. DCE-MRI images at the level of the 6.7 cm liver mass in segment VI (identified by white arrow) before (PRE) and after (POST) TACE treatment. The top row shows nonrim arterial phase hyperenhancement and nonperipheral "washout" during later phases, whereas the bottom row clearly shows tumor necrosis after treatment.

1. Introduction

Hepatocellular carcinoma (HCC) is responsible for 11% of all cancer-related deaths and ranks as the second leading cause of cancer mortality worldwide. In North America, HCC incidence and mortality rates are increasing [1]. Transarterial chemoembolization (TACE) is generally used with palliative intent or as a bridge to transplantation for non-metastatic HCC with T2 or T3 stage disease and no vascular involvement in patients who are not candidates for resection, ablation or transplantation [2,3].

HCCs are hypervascular tumors associated with a typical enhancement pattern observed on diagnostic imaging [4,5]. The growth and progression of such tumors are the result of changes in intranodular blood supply characterized by high arterial flow due to angiogenesis leading to unpaired neoarteries in the portal triad [6]. The Liver Imaging Reporting and Data System (LI-RADS) describes five major imaging features for the diagnosis of HCC on contrast-enhanced CT or MRI [5]. Of those, two imaging features refer to transient vascular phenomena observed on dynamic contrast-enhanced imaging: nonrim arterial phase hyperenhancement and nonperipheral "washout" during the portal venous and equilibrium phases (Fig. 1). Although there is an attempt to standardize interpretation of liver imaging, assessment of viable HCC and treatment response using such qualitative imaging characteristics remains subjective [5].

Furthermore, the accepted standard in assessing treatment response in HCC, the modified Response Evaluation Criteria in Solid Tumor (mRECIST), is based on contrast-enhanced CT or MRI acquired every 6–8 weeks after treatment [7], and relies on global *patient-level* assessment of changes in tumor size which usually occur 6–12 months after treatment [8]. However, an early *lesion-level* assessment of treatment response according to the LI-RADS v2018 Treatment Response algorithm, which takes into account the variable appearances of tumor after therapy for each lesion, is essential in planning additional therapy and can benefit patient outcome [8,9]. The LI-RADS Treatment Response algorithm, which incorporates concepts from mRECIST and European Association for the Study of the Liver (EASL) systems, relies on subjective visual assessment. DCE-MRI may provide objective and quantitative criteria to assess treatment response and differentiate nonviable from viable tumors in a shorter time period [10], as it offers a dynamic component to the evaluation of the viability of liver tumors which are not present in the standardized measurement.

The traditional approach for the diagnosis and assessment of treatment response of HCC has been to perform MRI with high spatial resolution, but low temporal resolution (i.e. 4–5 time points spaced 30–120 s apart). However, this approach relies on detection and qualitative analysis of residual vascularized portions of active HCC tumors. Another important concern with standard 3-phased MRI is that the arterial hepatic phase may overlap with portal venous enhancement due to the low temporal resolution. More recently, dynamic contrast-enhanced (DCE)-MRI providing higher temporal resolution with a minor trade-off in spatial resolution has been proposed to address this issue as it provides multiple arterial and venous phases [11]. Previous studies have shown that DCE-MRI can be used to derive objective quantitative metrics of viable HCC tumor using pharmacokinetic models that can supplement the subjective qualitative interpretation by radiologists, with minimal disruptions to clinical workflow [12–14]. This quantitative imaging technique, which measures changes in signal intensity due to local perfusion after injection of a gadolinium-based contrast agent, permits nonparametric and parametric analysis of tumor perfusion relative to background liver [15].

Recent DCE-MRI literature has assessed the efficacy of non-invasive evaluation of hepatic perfusion parameters. These studies either assessed DCE-MRI parameters in a cross-sectional [13,14] or longitudinal [8,16,17] approach by evaluating TACE only [13], TACE in combination with sunitinib [16], or sorafenib [17]. Most studies were prospective [13,14,16,17] and only a number of studies enrolled patients retrospectively [8,18]. These studies assessed tumor size [8] in addition to parametric [13,19], and non-parametric [8] analyses of tumor perfusion relative to background liver. We hypothesize that DCE-MRI parameters may provide objective quantitative biomarkers of HCC tumor response after TACE.

The purpose of this pilot study was to identify quantitative DCE-MRI perfusion parameters indicating tumor response of HCC to TACE. After performing a comprehensive literature review, we have integrated most DCE-MRI parameters reported in the literature for assessment of tumor response.

2. Materials and methods

2.1. Patients

This single-site prospective clinical trial (ClinicalTrials.gov reference number: NCT02878109) was approved by our institutional review board. All patients provided written and informed consent before

participating in the study.

Patients diagnosed by imaging with LI-RADS criteria demonstrating at least one tumor that is probably or definitely HCC (LR-4 or LR-5) and scheduled for TACE (targeted or segmental) treatment between June 2016 and June 2018 according to clinical indications were eligible for this study [20]. Subjects who were able to undergo an initial MRI 2 weeks prior to TACE and a follow-up examination 6 to 8 weeks after TACE were enrolled in this study if TACE was the only prescribed treatment. Patients who were previously enrolled but treated for new lesions could participate up to a maximum of two times in the study. All visible lesions on pre and post-treatment images were analyzed if the size exceeded 10 mm. These lesions could have been previously treated or not. Patients with liver transplant, morbid obesity, conditions preventing from undergoing a MRI (for instance, pacemaker, claustrophobia, or metal items in body), or for whom TACE was cancelled were excluded.

2.2. MR imaging protocol

Imaging was performed on a 3.0 T MRI system (Achieva TX, Philips Healthcare, Best, The Netherlands) using a 16-channel body array coil for signal reception. Patients were asked to fast for 4 h before the MRI scan to limit peristalsis. Prior to contrast injection, T1 mapping was performed using the variable flip-angle method with 3D mDixon acquisitions with flip angles of 4, 10, and 20° using the same acquisition parameters as for the dynamic contrast-enhanced sequence.

After injection of gadobenate dimeglumine (MultiHance®, Gd-BOPTA, Bracco Imaging SpA, Milan, Italy) with a dose adjusted according to patient weight (0.1 mmol/kg; maximum dose, 20 mL) and injected at 1 mL/s followed by a 15 mL saline flush at 2 mL/s, a dynamic 4D mDixon imaging scheme was used with a 10° flip angle. Images were acquired over 10 consecutive breath-holds at end-expiration extending up to approximately 5 min after injection, with imaging starting at 10 s after injection. All but the first breath-hold consisted of two keyhole acquisitions as well as an acquisition of the entire k-space, resulting in three temporal points per breath-hold (breath-hold duration of 13.7 s). Two extra keyhole acquisitions were performed for the first breath-hold generating five temporal points to ensure a better sampling of the arterial phase (breath-hold duration of 18.5 s). (Fig. 2) [21].

Imaging parameters were the following: repetition time (TR) of 4.1 ms, echo times (TE) of 1.27 and 2.6 ms, field of view (FOV) of $370 \times 300\ mm^2$, in-plane spatial resolution of $1.90 \times 1.90\ mm^2$, slice thickness of 5 mm, spacing between reconstructed slices of 2.5 mm, 100 reconstructed slices, receiver bandwidth of 960 Hz/pixel, and SENSE acceleration factor of 1.75. Water images after water/fat separation were used for interpretation. Temporal resolution for the keyhole acquisitions was 2.4 s, while the entire k-space acquisition took 8.9 s. The field-of-view of the sequence in the foot-head direction was 250 mm, which was enough to cover the liver in all cases.

2.3. MR imaging assessment of treatment response

Two fellowship-trained abdominal radiologists with experience in liver imaging (DO and AT, with 18 and 12 years of experience, respectively) independently reviewed the MRI examinations on picture archiving and communication system (PACS) workstations (Impax version 6.6, Agfa HealthCare, Mortsel, Belgium). MR imaging acquired before and after TACE of all included patients were examined to determine individual tumor response according to LI-RADS v2018 Treatment Response criteria [5]. The average time between baseline MRI and TACE was 15.7 ± 18.6 days with the maximum interval being 92 days. LI-RADS treatment response (LR-TR) categories include nonviable, equivocal, and viable. Disagreements on treatment response were solved by consensus two weeks after the individual interpretations. The consensus interpretation was based on a review of the imaging criteria and definitions provided in the LI-RADS Treatment Response documents and served as the reference standard for further nonparametric and parametric quantitative analysis. The standardized assessment form is provided in Supplemental material 1.

2.4. Blinding

Radiologists were blinded to the results of the DCE-MRI analysis and the image analyst performing quantitative analysis was blinded to treatment response assessment by radiologists.

2.5. MR image quantitative analysis

Four regions of interest (ROI) were manually selected in each set of images: the abdominal aorta, the portal vein, the non-tumoral liver parenchyma, and the liver tumors. The vascular phase that provided the best visualization of these structures was selected. To avoid error due to sampling, each 3D tumor was segmented on multiple slices after identification of tumors on bookmarked images by a second-year radiology resident (LB, with 1 year of experience), using Matlab R2016a (The MathWorks, Inc., Natick, MA, USA). The entire tumor, regardless of necrosis, was included in the segmentation to obtain a quantitative treatment response assessment unbiased by the radiologists' assessment of tumor viability. Verification of tumor segmentation was performed by a radiology fellow (MC, with 8 years of experience).

2.6. Non-rigid motion compensation

A motion compensation software (MoCo, Corstem, Montreal, Canada) was used to register all images on the different acquisition phases using non-rigid, subpixel deformation maps. The motion compensation software used interpolation warping functions following non-rigid displacement estimation based on an adapted optical flow formulation specifically amenable to perfusion series dynamics. This framework had the ability to register MRI perfusion image series with varying breathing patterns [22,23]. The implementation also featured automatic reference frame detection. Every ROI drawn was then automatically extended to all time points of motion compensated DCE-MRI in order to measure the average signal intensity versus time curves.

2.7. Nonparametric analysis

A nonparametric (model-free) analysis was performed on signal time curves after linear temporal interpolation to a time step of 1 s. This approach permits the direct calculation of simple perfusion measurements that correlate with tissue physiology. However, reproducibility is difficult because scanner type and settings as well as MR acquisition parameters can influence measurements of signal intensity [15]. These empirical parameters are illustrated in Fig. 3 and defined in Table 1.

2.8. Parametric analysis

Signal intensity at different time points for each ROI described above was converted to concentration of contrast agent using a linear conversion with T1 mapping [12]. A dual-input single-compartment model was fitted to experimental data of the tumor and surrounding liver tissue. This method requires a precise assessment of both the portal venous input function (PIF) and the arterial input function (AIF). The first was estimated from the concentration of contrast agent from the ROI in the portal vein (after linear temporal interpolation to 1 s). The second can be evaluated with high accuracy by using the gold standard method which consists of collecting arterial blood samples at various intervals and measuring the contrast agent concentration in plasma. Although effective, this technique is highly invasive and requires a lot of time and resources [24]. For these reasons, we opted for an indirect approach: an ROI drawn on the abdominal aorta at the level

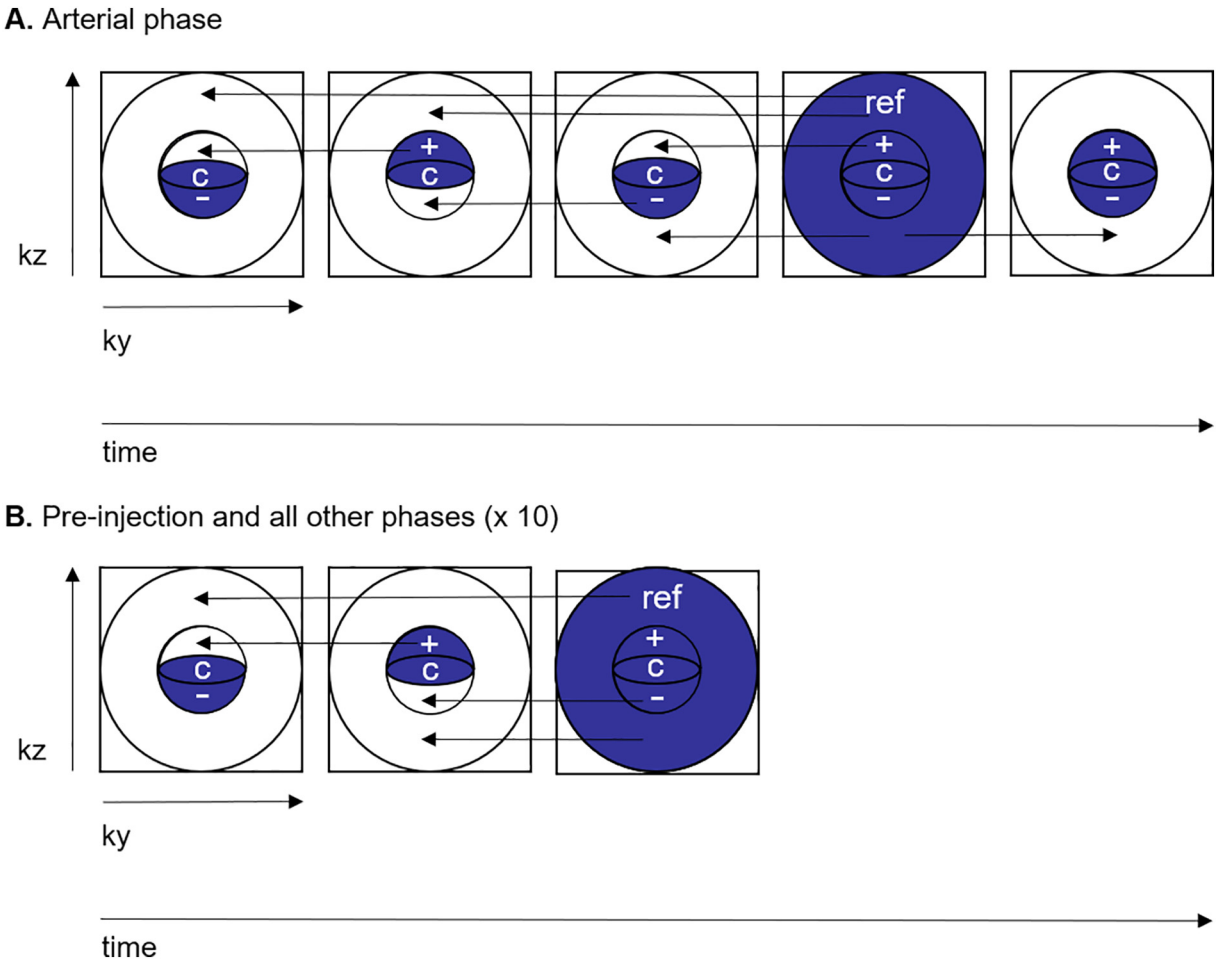

Fig. 2. DCE-MRI image acquisition scheme used for dynamic contrast-enhanced MRI. After contrast injection (a) five images and (b) three images were acquired per breath-hold for the arterial phase and the pre-injection and all other vascular phases, respectively. The fourth image was selected as the reference for the arterial phase to ensure that any motion at end breath-hold would not propagate to the other images. A keyhole center of one third of the full image resolution was used to achieve a good balance between dynamic contrast preservation and scan acceleration.

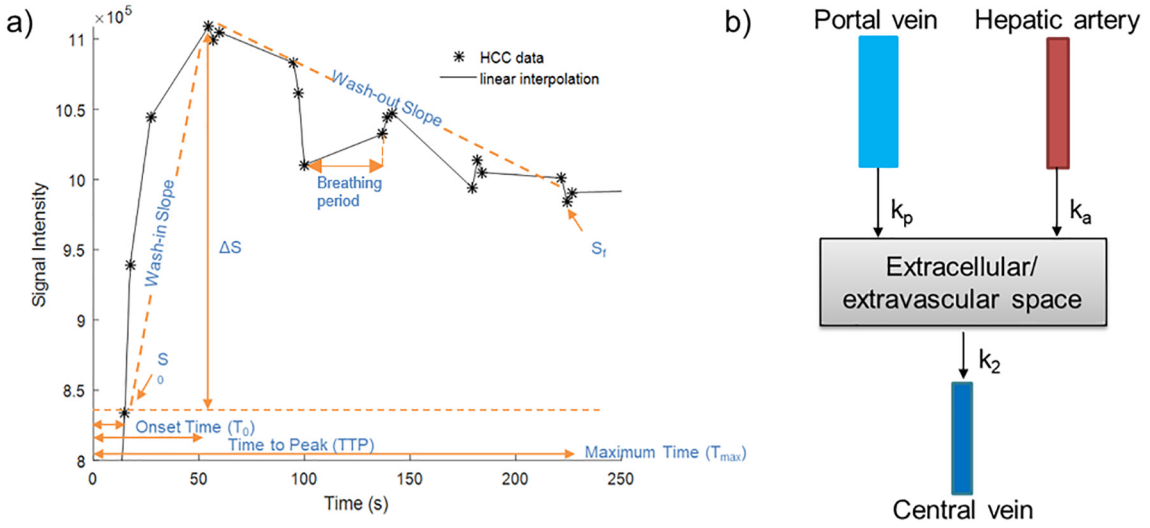

Fig. 3. (a) Example of signal intensity vs. time curve for HCC pre-TACE. (b) Schematic modeling of parameters extracted from a dual-input single-compartment model. k_a = transfer constant from the arterial plasma to the surrounding tissue, k_p = transfer constant from the portal venous plasma to the surrounding tissue, and k_2 = transfer constant from the tissue to the central vein. The average breathing period between breath-holds for our population was 31.0 s (range: 9.5–57.7 s).

Table 1
Definition of perfusion-related measurements extracted from nonparametric analysis of signal intensity vs time curves S(t). T_0 = onset time, TTP = time to peak, ΔS = peak enhancement, PER = peak enhancement ratio, and nMITR = normalized maximum intensity time ratio.

Measurement	Definition
T_0	Time of arrival of contrast agent in tissue
TTP	Time before contrast agent reaches its maximum value
ΔS	$S_{max} - S_0$, difference between maximum (S_{max}) and baseline (S_0) intensities
PER	$\frac{\Delta S}{S_0}$, relative peak enhancement
nMITR	$\frac{\Delta S}{TTP * S_0}$, normalized ratio between peak enhancement and TTP
Wash-in slope	$\frac{\Delta S}{TTP - T_0}$, slope connecting S_0 and S_{max} points
Wash-out slope	$\frac{S_{max} - S_f}{T_{max} - TTP}$, slope connecting S_{max} and final signal intensity (S_f) points

of the celiac trunk was selected as the arterial supply and signal intensity was converted to contrast agent concentration as described above. A combination of two Gaussians and an exponential modulated with a sigmoid function, as developed by Parker et al., was fitted to obtain a continuous AIF estimation [25]. The mean ratio between the arterial peak and the washout tail of the AIF was calculated from cases where the subject breath-hold pattern allowed to clearly image the first pass of contrast agent in the abdominal aorta. For cases where this was not possible due to first pass occurring during a breathing period, the maximum value of the experimental AIF was scaled to respect the same ratio. Therefore, our method was a compromise between using solely experimental data and a population averaged AIF, as previously demonstrated [26].

From the perfusion model described above, we were able to extract the transfer constants from the blood vessels to the surrounding extravascular extracellular space, k_a and k_p for the arterial plasma and the portal venous plasma respectively, and the transfer constant from the liver tissue to the central vein k_2 (Fig. 3) [27]. Using the relations developed by Materne et al., it was possible to deduce the tissue arterial fraction (ART), distribution volume (DV), and mean transit time (MTT) [12].

2.9. Statistical analysis

Statistical analyses were performed by a biostatistician (MC, 23 years of experience) (Software Stata/IC version 14.2). *P* values < 0.05 were considered significant for this pilot study.

2.9.1. Characteristics of patients and tumors

Descriptive statistics of baseline demographic and clinical data, including the etiology of liver disease, tumor characteristics, reference standard, and assessment of tumor response by radiologists, are summarized in Table 2. Categorical variables were expressed as numbers and percentages and continuous variables as mean ± standard deviation (SD), minimum and maximum.

2.9.2. Interreader agreement

Fleiss' kappa with 95% confidence intervals was used to determine interreader agreement between radiologists for assessment of treatment response. Agreement was interpreted as slight (0.01–0.2), fair (0.21–0.4), moderate (0.41–0.6), substantial (0.61–0.8), or almost perfect (0.81–1.0) [28].

2.9.3. Nonparametric and parametric analyses

Data were summarized as mean ± SD of parameters before and after TACE treatment for the non-viable and equivocal or viable groups. Comparisons of mean values within groups (before and after TACE treatment) were performed using nonparametric bootstrap (1000 sample) taking into account the clustering effect of lesions in patient. The change from baseline between groups was compared with the same approach and the 95% confidence intervals of change from baseline difference were reported. Lesions with clear necrosis after TACE were excluded from analysis for parameters that are fundamentally unreliable in the absence of enhancement: TTP, nMITR, wash-in, wash-out, k_a, k_p, k_2, MTT, DV, and ART. We did not perform correction for multiple comparisons because of the exploratory nature of this pilot study. The area under the receiver operating characteristic (ROC) curve for each parameter was also estimated using nonparametric bootstrap taking into account the clustering effect.

Table 2
Characteristics of patients and tumors.

Characteristics	Data
Sex	
Male	25/28 (89.3)
Female	3/28 (9.5)
Age (y)	
Median (range)	65.2 (51–76)
Known cirrhosis	26/28 (92.9)
Etiology of liver disease	
Hepatitis C infection	11/28 (39.3)
Hepatitis B infection	1/28 (3.6)
Alcoholic liver disease	12/28 (42.9)
Non-alcoholic steatohepatitis	10/28 (35.7)
Child Pugh score	
A	17/28 (60.7)
B	7/28 (25.0)
C	0/28 (0)
Not available in patient file	4/28 (14.3)
Number of HCCs per patient	
Mean (range)	2 (1–6)
HCC size (mm)	
Mean ± SD (range)	26.2 ± 19.3 (10–104)
Treatment	
Conventional TACE	25/28 (89.3)
DEB-TACE	3/28 (10.7)
Chemotherapeutic agents	
Adriamycine	16/28 (57.1)
Doxorubicine	12/28 (42.9)
Embolizing agents	
GelFoam	7/28 (25.0)
BeadBlocks	13/28 (46.4)
DC beads	2/28 (7.1)
Combination	3/28 (10.7)
Not specified	3/28 (10.7)
Tumor viability according to radiologists	
Nonviable	27/52 (51.9)
Equivocal or viable	25/52 (48.1)
Deceased	6/28 (21.4)

Note. — Data are numerator and denominator. Data in parentheses are percentages unless stated otherwise.

2.9.4. Diagnostic performance of selected parameter

The area under the ROC curves was calculated as an effect size to determine which perfusion parameter best discriminated tumor viability.

3. Results

3.1. Characteristics of patients and tumors

Twenty-eight patients totaling 52 HCCs with size ranging from 10 to 104 mm were included in this pilot study. The flowchart of patient selection is shown in Fig. 4 and characteristics of patients and tumors in

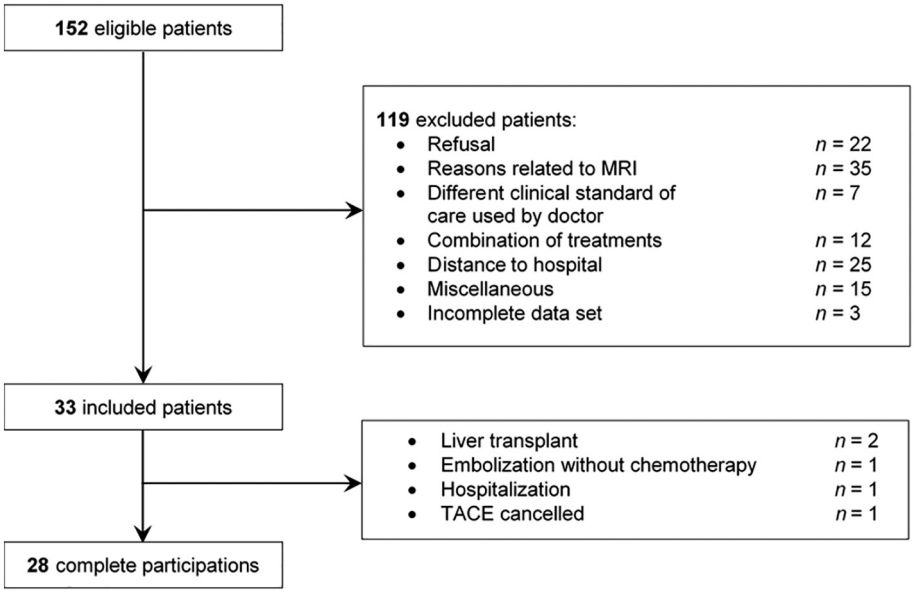

Fig. 4. Flowchart of patient selection.

Table 2. Individuals diagnosed with HCC and awaiting TACE treatment between June 2016 and June 2018 were eligible for this study ($n = 152$). Of those, 119 patients were excluded. The three most common reasons for patient exclusion were related to MRI, refusal, and distance from hospital. Thus, a total of 33 patients were included, but five could not complete their participation due to liver transplantation ($n = 2$), bland embolization ($n = 1$), medical emergency requiring hospitalization ($n = 1$), and TACE cancellation ($n = 1$). Fifty-two lesions were included, but nine were excluded from quantitative analysis due to necrosis for parameters listed above.

3.2. Interreader agreement

Interreader agreement between radiologists for assessment of treatment response using LI-RADS v2018 treatment response criteria was moderate ($\kappa = 0.50 \pm 0.11$, proportion of observed agreement = 0.72).

3.3. Nonparametric and parametric analyses

Fig. 5 shows global enhancement curves for the abdominal aorta, the portal vein, the liver and the tumor before and after chemoembolization for nonviable and equivocal or viable tumors. HCCs present arterial phase hyperenhancement and washout in both groups before treatment. Of note, the degree of enhancement is higher and timing of peak arterial enhancement occurs earlier in equivocal or viable tumors than in nonviable tumors. Furthermore, after TACE treatment, enhancement decreased in the group with LR-TR nonviable tumors, whereas enhancement remained slightly higher than that of the background liver during the arterial phase for LR-TR equivocal or viable tumors.

Comparison between groups (nonviable vs. equivocal or viable tumors) at baseline and after treatment is summarized in Table 3. For nonviable tumors, time to peak increased after treatment ($p < 0.01$). For equivocal or viable tumors, the TTP and MTT significantly increased ($p < 0.01$ and $p = 0.01$, respectively) and k_2 significantly decreased after treatment ($p = 0.01$).

The size of equivocal or viable tumors was 26.2 ± 20.3 mm before and 20.3 ± 18.3 mm after TACE ($p < 0.01$). The size of nonviable tumors was 18.7 ± 6.5 mm before and 15.0 ± 5.2 mm after TACE ($p < 0.01$) (Table 3).

4. Discussion

This prospective clinical study identified quantitative DCE-MRI perfusion parameters for assessing tumor response of HCC to TACE. All patients had at least one malignant tumor (probably or definitely HCC) confirmed by previous diagnostic imaging and were scheduled for TACE treatment. MRI examinations were interpreted independently and in consensus by radiologists to determine individual tumor response according to LI-RADS v2018 treatment response criteria.

Of note, the interreader agreement for assessment of treatment response to TACE using LI-RADS v2018 treatment response criteria was moderate. This level of agreement was slightly lower than previously reported and confirmed the need for an objective and preferably quantitative technique for assessing treatment response. Donati et al. reported interreader agreement ranging from moderate to substantial ($\kappa = 0.56–0.80$) for assessment of treatment response to TACE in 74 patients with HCC using mRECIST [29].

We found that TTP significantly increased after treatment for nonviable tumors. TTP and MTT also increased and k_2 decreased after treatment for equivocal or viable tumors. Prior to chemoembolization, HCC hyperenhancement occurs earlier than in the non-tumoral hepatic parenchyma due to increased arterialization of the tumor. After chemoembolization of the tumor feeding arteries, the treated tumor—-which depended on neoarteries for its blood supply—enhances lower and later relative to the adjacent liver which enhances due to its preserved portal venous supply [6]. The increase in TTP probably reflects these physiological changes in tumor perfusion [30]. However, increase in TTP may only be due to reduced arterial hyperenhancement without indicating non-viability. Thus, this should be further investigated in future and larger studies. Of note, nine nonviable lesions with complete necrosis were excluded from quantitative analysis for a majority of parameters due to an absence of visible enhancement, which precludes the estimation of reliable perfusion parameters. The exclusion of these cases with clear positive treatment response could in part explain why changes in parameters were not significantly different between the groups since only lesions showing at least some enhancement were analyzed.

Furthermore, global perfusion curves show that the enhancement of equivocal or viable tumors occurs earlier than for nonviable tumors before treatment. This may suggest that lesions that are highly arterialized before TACE remain active after treatment. Hence, timing of HCC enhancement may predict tumor treatment outcome. However,

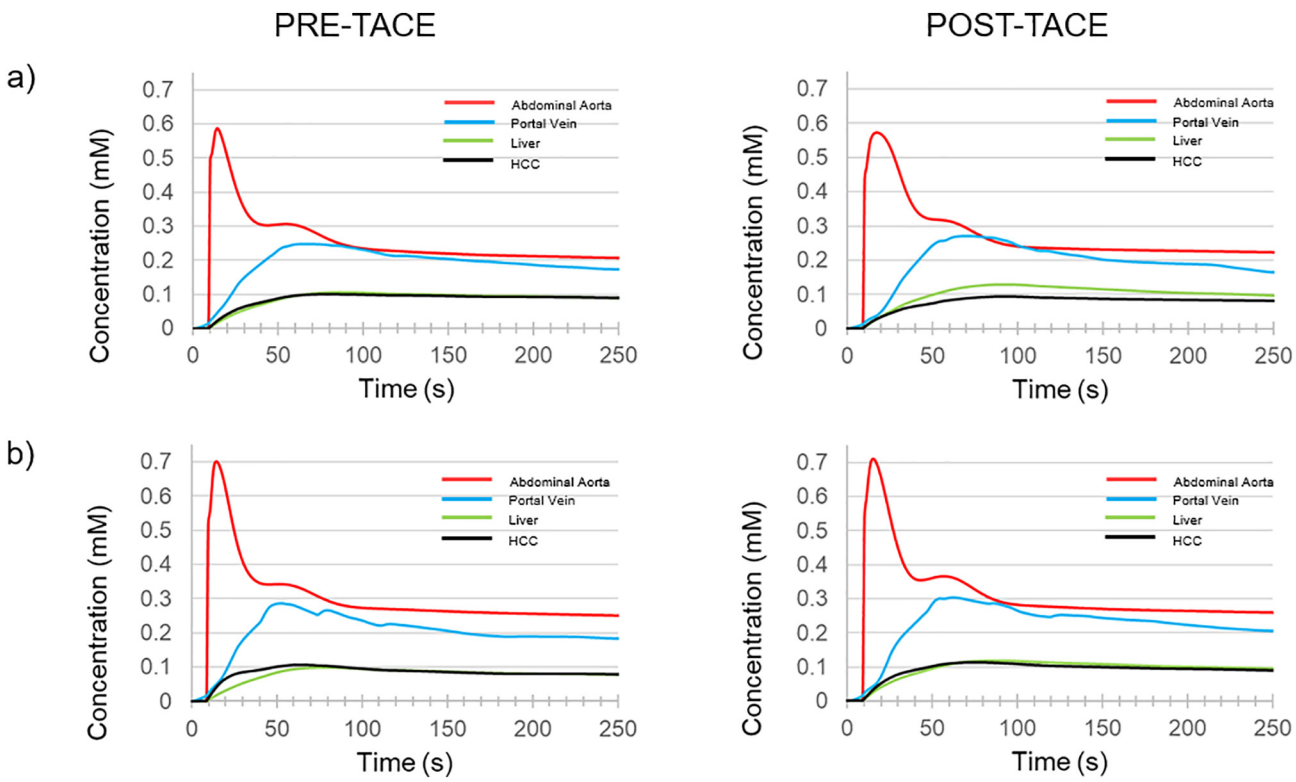

Fig. 5. Averaged concentration vs. time curves for (a) 27 nonviable and (b) 25 equivocal or viable tumors. Red curve = abdominal aorta, blue curve = portal vein, green curve = liver, black curve = hepatocellular carcinoma. Differences in sequence timing between the subjects have been compensated before averaging. (For interpretation of the references to colour in this figure legend, the reader is referred to the web version of this article.)

current clinical dynamic contrast-enhanced sequences do not have sufficiently high temporal resolution to detect this difference in enhancement timing.

As expected, the arterial fraction in tumors before treatment (0.4) was higher than values typically reported for normal liver parenchyma in the literature (0.25) [31] as the arterial blood supply to HCC increases due to angiogenesis [32]. Similarly, Marquez et al. found that HCCs in 24 patients showed a higher arterialization before doxorubicin-eluted bead based TACE treatment [33].

Taouli et al., using DCE-MRI to quantify perfusion in HCC and surrounding liver parenchyma, reported that the arterial fraction, the arterial hepatic blood flow and the distribution volume decreased and the portal venous hepatic blood flow increased in three patients with HCC who underwent TACE treatment [13]. However, their study reported no significant change in MTT. Of note, ROIs were drawn on the enhancing part or the lesion, unlike our study which included the entire

Table 3
Baseline characteristics and changes in parameters after TACE.

Parameters (for tumors)	Nonviable (n = 27/52)			Equivocal or viable (n = 25/52)			Comparison at baseline	Nonviable vs equivocal or viable
	Before treatment	After treatment	p value	Before treatment	After treatment	p value	p value	p value
Tumor size (mm)	18.7 ± 6.5	15.0 ± 5.2	< **0.01**	26.2 ± 20.3	20.3 ± 18.3	< **0.01**	0.08	0.74
Nonparametric analysis								
PER	0.9 ± 0.4	0.8 ± 0.9	0.64	1.0 ± 0.4	1.0 ± 0.5	0.74	0.59	0.53
TTP (s)*	62.5 ± 18.2	83.3 ± 12.8	< **0.01**	54.4 ± 24.1	69.5 ± 18.9	< **0.01**	0.28	0.47
nMITR, 10^{-2} (s^{-1})*	1.7 ± 1.2	1.3 ± 1.1	0.34	2.1 ± 1.7	1.5 ± 0.7	0.16	0.45	0.73
Wash-in, 10^{3} (s^{-1})*	27.5 ± 25.3	19.9 ± 13.4	0.16	31.2 ± 30.2	25.7 ± 19.1	0.50	0.70	0.83
Wash-out, 10^{2} (s^{-1})*	10.1 ± 14.9	13.7 ± 25.2	0.42	13.6 ± 10.4	16.4 ± 19.6	0.52	0.36	0.89
Parametric analysis								
k_a, 10^{-3} (s^{-1})*	4.4 ± 4.7	5.6 ± 7.6	0.64	4.8 ± 4.4	6.9 ± 10.2	0.28	0.79	0.68
k_p, 10^{-3} (s^{-1})*	8.0 ± 9.7	11.7 ± 18.2	0.29	20.4 ± 65.2	5.1 ± 5.5	0.25	0.36	0.20
k_2, 10^{-2} (s^{-1})*	13.4 ± 14.4	8.9 ± 15.0	0.43	14.8 ± 14.1	8.1 ± 9.1	**0.01**	0.67	0.64
MTT (s)*	36.0 ± 51.6	43.1 ± 35.2	0.46	14.2 ± 11.8	33.9 ± 36.8	**0.01**	0.10	0.33
DV (%)*	32.5 ± 47.9	45.2 ± 41.5	0.30	42.9 ± 123.6	48.6 ± 124.1	0.87	0.70	0.84
ART*	0.4 ± 0.3	0.4 ± 0.3	0.93	0.4 ± 0.2	0.5 ± 0.3	0.13	0.71	0.39

All values except P values are expressed as mean ± SD. PER = peak enhancement ratio, TTP = time to peak, nMITR = normalized maximum intensity time ratio, k_a = transfer constant from the arterial plasma to the surrounding tissue, k_p = transfer constant from the portal venous plasma to the surrounding tissue, k_2 = transfer constant from the tissue to the central vein, MTT = mean transit time, DV = distribution volume and ART = arterial fraction. * Non-viable lesions with clear necrosis after TACE (n = 9) were excluded from analysis for these parameters due to the absence of visible enhancement.
Bold text was used to highlight significant results (p value > 0.05)

tumor regardless of necrosis in 28 patients with a total of 52 tumors. This difference in the ROI placement method may explain differences between our studies. The authors also reported that untreated HCC ($n = 16$) had a significantly higher arterial fraction and a lower portal venous hepatic blood flow than treated lesions ($n = 17$).

Pahwa et al. noted a statistically significant difference in arterial fraction and distribution volume in 28 HCCs compared to healthy liver tissue in volunteers [14]. The authors also found that there was no significant difference in MTT. Again, ROIs were only drawn on the enhancing part of the tumor. Parameters were obtained by fitting a similar dual-input single-compartment model to data of contrast concentration. Images were acquired using a 3D free breathing spiral acquisition with a temporal resolution of 1.6 to 1.9 s. This enabled a more accurate evaluation of the arterial and venous input functions.

In a study of patients with unresectable primary liver cancer (26 intrahepatic cholangiocarcinomas and 8 HCCs), Jarnagin et al. found that changes in perfusion characteristics shortly after hepatic arterial infusion with floxuridine and dexamethasone may predict treatment outcome [19]. A dual-compartment general kinetic model was used to calculate perfusion parameters. Voxel analyses of the top decile values within the ROI showed a survival correlation.

In a retrospective study on 48 patients with 71 HCCs, Bonekamp et al. [8] found that decrease in venous enhancement one month after TACE differed significantly between partial response, stable disease and progressive disease as assessed by using RECIST six months after treatment. Venous enhancement was calculated as a percentage of contrast-enhanced values without using a perfusion model. However, we did not confirm significant differences in venous enhancement by using a dual-input perfusion model.

Using the one-compartment Tofts model, Pokuri et al. [16] assessed DCE-MRI biomarkers of treatment response to sunitinib and TACE combination therapy in 16 patients with HCC. The authors found that the transfer constant (K_{trans}) and viable tumor percentage after combination therapy decreased significantly. Similarly, Saito et al. [17] assessed changes in perfusion parameters after TACE combined with sorafenib in 11 patients with 21 HCCs and found that K_{trans} was significantly reduced post-treatment in the responder group. They also noted that DV significantly decreased in responders at three and 10 days after treatment, whereas decrease in DV was not significant in non-responders. In contrast, we found a non-significant increase in DV in both groups. However, we used a different definition of DV that relied on k_a, k_p and k_2 instead of K_{trans}.

Our pilot study had some limitations. First, this pilot study had a small sample. However, this is the largest study so far to perform paired comparisons before and after TACE. Future studies with larger sample size will be required to identify thresholds for DCE-MRI parameters that indicate significant tumor response. Second, the peak arterial enhancement may not have been consistently acquired due to an early or late acquisition in the arterial phase resulting from the use of a sequence performed over multiple breath-holds. This may have introduced errors in the modelling of the arterial input function and early tumor enhancement [34]. In the future, free breathing acquisitions with radial k-space sampling that provide uniform temporal resolution and robustness to organ motion may allow continuous assessment of the time-intensity curve throughout the examination, including during the arterial peak [35]. Furthermore, we acknowledge that the lack of independent reference standard constitutes a limitation of our study. However, over the past two decades, the definite diagnosis of HCC and the assessment of treatment response have been largely based on imaging. Nowadays, liver biopsy is not mandated to confirm the diagnosis of HCC or viable tumor. Further, it would be unethical to confirm tumor recurrence with follow-up imaging and withholding treatment in patients with intermediate-stage HCC with a high pre-test likelihood of HCC. Therefore, the use of clinical interpretation as the reference standard was inevitable in our patient cohort. Our study included lesions that had previously been treated by TACE. However, this was on a small number of lesions and patients (6 and 4, respectively). Finally, we used a dual-input single-compartment model to fit the concentration curves using simple assumptions. Some authors have proposed more complex dual-input dual-compartment models [36] or distribution parameter models [37] to reflect liver perfusion and contrast distribution. However, there is still scarce evidence that these models can be applied to HCCs or that parameters derived from these models would provide better classification accuracy.

In conclusion, this prospective pilot study showed that time to peak significantly changed after TACE treatment for both groups. Other parameters such as k_2 and MTT changed only in the equivocal or viable group although the difference with the nonviable group was not significant. These promising results support the conduct of further studies with larger cohort size and clinical outcomes to test whether DCE-MRI with better temporal resolution by means of innovative free-breathing techniques can predict tumor response following TACE procedures in HCC patients.

Supplementary data to this article can be found online at https://doi.org/10.1016/j.mri.2019.06.017.

Institution from which the work originated

Centre de Recherche du Centre Hospitalier de l'Université de Montréal (CRCHUM).
900, rue Saint-Denis (Tour Viger).
Montreal, Qc, Canada, H5B 1B2.

Presentation

An earlier version of this work was presented at:
ISMRM 2018, Paris, France. Poster. #2623
Dynamic Contrast-Enhanced MRI to Assess Hepatocellular Carcinoma Response to Transarterial Chemoembolization: a Pilot Study.
Thibodeau-Antonacci A, Petitclerc L, Gilbert G, Bilodeau L, Castel H, Turcotte S, Olivié D, Huet C, Perreault P, Soulez P, Tang A, Kadoury S.

Presentation

This paper was not presented at a previous meeting or submitted for presentation at a future meeting.

Funding

This work was funded by an Operating Grant from the Canadian Institutes of Health Research (CIHR) (#340909) to Samuel Kadoury (PI), a Clinical Research Scholarship – Junior 1 Salary Award from the Fonds de Recherche du Québec - Santé (FRQS-ARQ) to Simon Turcotte and a Junior 2 Salary Award from the Fonds de recherche du Québec - Santé and the Fondation de l'association des Radiologists du Québec (FRQS-ARQ #34939) to An Tang.

Acknowledgments

N/A.

References

[1] Tang A, Hallouch O, Chernyak V, Kamaya A, Sirlin CB. Epidemiology of hepatocellular carcinoma: target population for surveillance and diagnosis. Abdom Radiol (NY) 2018;43(1):13–25.
[2] Heimbach JK, Kulik LM, Finn RS, Sirlin CB, Abecassis MM, Roberts LR, et al. AASLD guidelines for the treatment of hepatocellular carcinoma. Hepatology 2018;67(1):358–80.
[3] Marrero JA, Kulik LM, Sirlin CB, Zhu AX, Finn RS, Abecassis MM, Roberts LR, Heimbach JK. Diagnosis, staging and management of hepatocellular carcinoma: 2018 Practice Guidance by the American Association for the Study of Liver Diseases. PMID: 29624699 Hepatology 2018;68(2):723–50. https://doi.org/10.1002/hep.

29913.
[4] Tang A, Bashir MR, Corwin MT, Cruite I, Dietrich CF, Do RKG, et al. Evidence supporting LI-RADS major features for CT- and MR imaging-based diagnosis of hepatocellular carcinoma: a systematic review. Radiology 2018;286(1):29–48.
[5] American College of Radiology. Liver imaging reporting and data system URL consulted https://www.acr.org/Clinical-Resources/Reporting-and-Data-Systems/LI-RADS.
[6] Park YN, Yang CP, Fernandez GJ, Cubukcu O, Thung SN, Theise ND. Neoangiogenesis and sinusoidal "capillarization" in dysplastic nodules of the liver. Am J Surg Pathol 1998;22(6):656–62.
[7] Schwartz LH, Litiere S, de Vries E, Ford R, Gwyther S, Mandrekar S, et al. RECIST 1.1-update and clarification: from the RECIST committee. Eur J Cancer 2016;62:132–7.
[8] Bonekamp S, Jolepalem P, Lazo M, Gulsun MA, Kiraly AP, Kamel IR. Hepatocellular carcinoma: response to TACE assessed with semiautomated volumetric and functional analysis of diffusion-weighted and contrast-enhanced MR imaging data. Radiology 2011;260(3):752–61.
[9] Kielar A, Fowler KJ, Lewis S, Yaghmai V, Miller FH, Yarmohammadi H, et al. Locoregional therapies for hepatocellular carcinoma and the new LI-RADS treatment response algorithm. Abdom Radiol (NY) 2018;43(1):218–30.
[10] Chen BB, Shih TT. DCE-MRI in hepatocellular carcinoma-clinical and therapeutic image biomarker. World J Gastroenterol 2014;20(12):3125–34.
[11] Coenegrachts K. Magnetic resonance imaging of the liver: new imaging strategies for evaluating focal liver lesions. World J Radiol 2009;1(1):72–85.
[12] Materne R, Smith AM, Peeters F, Dehoux JP, Keyeux A, Horsmans Y, et al. Assessment of hepatic perfusion parameters with dynamic MRI. Magn Reson Med 2002;47(1):135–42.
[13] Taouli B, Johnson RS, Hajdu CH, Oei MT, Merad M, Yee H, et al. Hepatocellular carcinoma: perfusion quantification with dynamic contrast-enhanced MRI. AJR Am J Roentgenol 2013;201(4):795–800.
[14] Pahwa S, Liu H, Chen Y, Dastmalchian S, O'Connor G, Lu Z, et al. Quantitative perfusion imaging of neoplastic liver lesions: a multi-institution study. Sci Rep 2018;8(1):4990.
[15] Khalifa F, Soliman A, El-Baz A, Abou El-Ghar M, El-Diasty T, Gimel'farb G, et al. Models and methods for analyzing DCE-MRI: a review. Med Phys 2014;41(12):124301.
[16] Pokuri VK, Tomaszewski GM, Ait-Oudhia S, Groman A, Khushalani NI, Lugade AA, et al. Efficacy, safety, and potential biomarkers of sunitinib and transarterial chemoembolization (TACE) combination in advanced hepatocellular carcinoma (HCC): phase II trial. Am J Clin Oncol 2018;41(4):332–8.
[17] Saito K, Ledsam J, Sugimoto K, Sourbron S, Araki Y, Tokuuye K. DCE-MRI for early prediction of response in hepatocellular carcinoma after TACE and sorafenib therapy: a pilot study. J Belg Soc Radiol 2018;102(1):40.
[18] O'Connor JP, Rose CJ, Jackson A, Watson Y, Cheung S, Maders F, et al. DCE-MRI biomarkers of tumour heterogeneity predict CRC liver metastasis shrinkage following bevacizumab and FOLFOX-6. Br J Cancer 2011;105(1):139–45.
[19] Jarnagin WR, Schwartz LH, Gultekin DH, Gonen M, Haviland D, Shia J, et al. Regional chemotherapy for unresectable primary liver cancer: results of a phase II clinical trial and assessment of DCE-MRI as a biomarker of survival. Ann Oncol 2009;20(9):1589–95.
[20] Gaba RC, Lokken RP, Hickey RM, Lipnik AJ, Lewandowski RJ, Salem R, et al. Quality improvement guidelines for transarterial chemoembolization and embolization of hepatic malignancy. Journal of vascular and interventional radiology: JVIR 2017;28(9):1210–23 e3.
[21] Coenegrachts K, Ghekiere J, Denolin V, Gabriele B, Herigault G, Haspeslagh M, et al. Perfusion maps of the whole liver based on high temporal and spatial resolution contrast-enhanced MRI (4D THRIVE): feasibility and initial results in focal liver lesions. Eur J Radiol 2010;74(3):529–35.
[22] Jacobs M, Benovoy M, Chang LC, Arai AE, Hsu LY. Evaluation of an automated method for arterial input function detection for first-pass myocardial perfusion cardiovascular magnetic resonance. J Cardiovasc Magn Reson 2016;18:17.
[23] Benovoy M, Jacobs M, Cheriet F, Dahdah N, Arai AE, Hsu LY. Robust universal nonrigid motion correction framework for first-pass cardiac MR perfusion imaging. J Magn Reson Imaging 2017;46(4):1060–72.
[24] Sari H, Erlandsson K, Thielemans K, Atkinson D, Arridge S, Ourselin S, et al. Incorporation of MRI-AIF information for improved kinetic modelling of dynamic PET data. EJNMMI Phys 2014;1(Suppl. 1):A43.
[25] Parker GJ, Roberts C, Macdonald A, Buonaccorsi GA, Cheung S, Buckley DL, et al. Experimentally-derived functional form for a population-averaged high-temporal-resolution arterial input function for dynamic contrast-enhanced MRI. Magn Reson Med 2006;56(5):993–1000.
[26] Hormuth 2nd DA, Skinner JT, Does MD, Yankeelov TE. A comparison of individual and population-derived vascular input functions for quantitative DCE-MRI in rats. Magn Reson Imaging 2014;32(4):397–401.
[27] Wang H, Cao Y. Correction of arterial input function in dynamic contrast-enhanced MRI of the liver. J Magn Reson Imaging 2012;36(2):411–21.
[28] Landis JR, Koch GG. The measurement of observer agreement for categorical data. Biometrics 1977;33(1):159–74.
[29] Donati OF, Do RK, Hotker AM, Katz SS, Zheng J, Moskowitz CS, et al. Interreader and inter-test agreement in assessing treatment response following transarterial embolization for hepatocellular carcinoma. Eur Radiol 2015;25(9):2779–88.
[30] Ippolito D, Bonaffini PA, Ratti L, Antolini L, Corso R, Fazio F, et al. Hepatocellular carcinoma treated with transarterial chemoembolization: dynamic perfusion-CT in the assessment of residual tumor. World J Gastroenterol 2010;16(47):5993–6000.
[31] Banerji A, Naish JH, Watson Y, Jayson GC, Buonaccorsi GA, Parker GJ. DCE-MRI model selection for investigating disruption of microvascular function in livers with metastatic disease. J Magn Reson Imaging 2012;35(1):196–203.
[32] International Consensus Group for Hepatocellular NeoplasiaThe International Consensus Group for Hepatocellular N. Pathologic diagnosis of early hepatocellular carcinoma: a report of the international consensus group for hepatocellular neoplasia. Hepatology 2009;49(2):658–64.
[33] Marquez HP, Karalli A, Haubenreisser H, Mathew RP, Alkadhi H, Brismar TB, et al. Computed tomography perfusion imaging for monitoring transarterial chemoembolization of hepatocellular carcinoma. Eur J Radiol 2017;91:160–7.
[34] Jajamovich GH, Calcagno C, Dyvorne HA, Rusinek H, Taouli B. DCE-MRI of the liver: reconstruction of the arterial input function using a low dose pre-bolus contrast injection. PLoS One 2014;9(12):e115667.
[35] Feng L, Grimm R, Block KT, Chandarana H, Kim S, Xu J, et al. Golden-angle radial sparse parallel MRI: combination of compressed sensing, parallel imaging, and golden-angle radial sampling for fast and flexible dynamic volumetric MRI. Magn Reson Med 2014;72(3):707–17.
[36] Saito K, Ledsam J, Sourbron S, Otaka J, Araki Y, Akata S, et al. Assessing liver function using dynamic Gd-EOB-DTPA-enhanced MRI with a standard 5-phase imaging protocol. J Magn Reson Imaging 2013;37(5):1109–14.
[37] Koh TS, Thng CH, Lee PS, Hartono S, Rumpel H, Goh BC, et al. Hepatic metastases: in vivo assessment of perfusion parameters at dynamic contrast-enhanced MR imaging with dual-input two-compartment tracer kinetics model. Radiology 2008;249(1):307–20.